An Approach to Combine Balancing with Hierarchical Whole-Body Control for Legged Humanoid Robots

Bernd Henze, Alexander Dietrich, and Christian Ott

***Abstract*—Legged humanoid robots need to be able to perform a variety of tasks including interaction with the environment while maintaining the balance. The external wrenches, which arise from the physical interaction, must be taken into account in order to achieve robust and compliant balancing. This work presents a new control approach for combining multiobjective hierarchical control based on null space projections with passivity-based multi-contact balancing for legged humanoid robots. In order to achieve a proper balancing, all task forces/torques are first distributed to the end effectors and then mapped into joint space considering the task hierarchy. The control approach is evaluated both in simulation and experiment with the humanoid robot TORO.**

***Index Terms*—Compliance and impedance control, force control, humanoid robots, redundant robots.**

I. Introduction

HUMANOID robots are predestined for service robotic applications, industrial manufacturing or disaster scenarios, as the tasks are often monotonic, physically demanding or too dangerous for humans. To cope with these scenarios, two requirements are of special importance: first, the robot must be capable of moving in unstructured environments which includes climbing stairs or ladders, moving in confined spaces, or overcoming general obstacles and debris. In order to improve the robustness in this terrain, the system can utilize multiple end effectors (e.g., the hands in addition to the feet) to gain a wider and more stable support. Second, the robot must be capable of interacting with the environment by e.g. performing a manipulation task such as opening a door or lifting an object. Usually, that implies several simultaneous objectives to be followed such as self-collision avoidance, the avoidance of singular configurations, the observation of the environment, and so on. The challenge with such a variety of tasks is that they might conflict and consequently interfere with each other. That problem can be solved by the approach of null-space-based multi-objective control.

One can find multiple types of approaches for dealing with the problem of multi-contact balancing. A versatile approach is offered by the field of whole-body control considering all Degrees of Freedom (DoFs) of the robot as e.g. by using inverse kinematics or inverse dynamics. For instance in [1], a dynamic balance force controller is presented for computing joint torques based on a desired CoM (Center of Mass) trajectory and some task wrenches. In [2] an orthogonal decomposition is used in order to obtain a solution for the inverse dynamics without the need for information on the contact forces. The decomposition was then reused in [3] to minimize the constraint forces. In [4] a framework is presented for the optimization of the CoP (Center of Pressure) in each foot. In [5] the concept of virtual linkage is used to describe internal forces and the resultant wrench on the CoM which is integrated into a prioritized multitasking controller for whole-body control. In [6], the authors present a balancing approach based on momentum control by hierarchically solving the inverse dynamics. The algorithm is thoroughly analyzed with a wide variety of experiments.

A passivity-based approach for compliant balancing of humanoid robots was first proposed in [7] by computing suitable ground-applied forces which are mapped to the joint torques. This idea was reused in [8] exploiting the fact that the problems of balancing and grasping are structurally similar. The work [8] was extended in [9] to handle multiple contacts in combination with a feedforward control leading to a structure of the closed-loop system similar to classical PD+ control [10].

Since the robot has to fulfill a variety of tasks including balancing, the concept of hierarchical multi-task control can be employed, in which one usually distinguishes between two

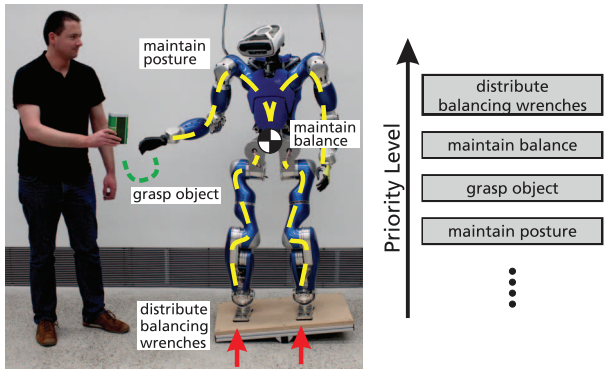

Fig. 1. Example for multi-objective control while balancing on multiple contacts.

Manuscript received August 31, 2015; accepted December 12, 2015. Date of publication December 29, 2015; date of current version February 29, 2016. This paper was recommended for publication by Associate Editor L. Righetti and Editor N. Tsagarakis upon evaluation of Reviewers' comments. This work was supported in part by the Helmholtz Association under Grant VH-NG-808 and in part by the European Commission under Grant H2020-ICT-645097 COMANOID.

The authors are with the German Aerospace Center (DLR), Institute of Robotics and Mechatronics, 82234 Wessling, Germany (e-mail: bernd.henze@dlr.de; alexander.dietrich@dlr.de; christian.ott@dlr.de).

Digital Object Identifier 10.1109/LRA.2015.2512933

basic approaches: first, an optimization problem is formulated and numerically solved such as in [11], [12]. Second, so-called null space projections [13], [14], [15], [16] are used to prioritize the tasks on control level by establishing a strict hierarchy among them. While the optimization is beneficial due to the easy incorporation of inequality constraints, null space approaches have the advantages of being numerically cheap and confirmed by formal proofs of stability [17], [18]. Especially the last aspect is of major importance in physical human-robot-interaction.

The task hierarchy is realized by projecting a lower-priority control action in the null space of all higher priority tasks. This implies that the subordinate tasks may not disturb the more important ones, but the more important ones may suspend the subordinate tasks, if necessary. This scheme can be iteratively applied until an arbitrarily complex task hierarchy is established. Possible subtasks in such a hierarchy are Cartesian impedance and singularity avoidance [19], joint limit avoidance [20], or collision avoidance [21], [22], for example. In the literature, there already exist several well-established frameworks, which are based on these techniques. While most of them have been confirmed in simulations [23], [24], the availability of modern humanoid robots has given a strong impetus to the experimental validation [25], [26], [27], [28].

This letter extends the work of [17] and [9] by combining torque-based multi-contact balancing with hierarchical multi-task control, see Fig. 1. In [17] a task prioritization is presented for handling multiple objectives as they occur for the serial kinematics of a redundant robotic manipulator. The balancing controller presented in [9] offers a framework for dealing with the force distribution problem for the multiple contacts of a branched kinematic chain in a hierarchical way. One advantage of the presented approach is that we apply a numeric optimization only for solving the force distribution problem, where it is necessary. The hierarchy concerning the serial kinematics is implemented using null space projectors, which is numerically cheap and allows us to prove asymptotic stability as shown in [17]. Furthermore, the presented approach is explicitly designed for handling external disturbances without the necessity of measuring them.

The letter is organized as follows: in Sec. II, the original null-space-based task hierarchy is recapitulated (Sec. II-A) and the new approach is synthesized (Sec. II-C). Stability is discussed in Sec. II-D and the link to the optimization-based balancing algorithm is presented in Sec. II-F. Experiments are conducted on the humanoid robot TORO in Sec. III, and the discussion of the results closes the letter in Sec. IV.

II. Theory

A. Recapitulation of the Task Hierarchy [17]

The dynamics of a robot with n DoF can be formulated as

$$\boldsymbol{M}(\boldsymbol{q})\ddot{\boldsymbol{q}} + \boldsymbol{C}(\boldsymbol{q},\dot{\boldsymbol{q}})\dot{\boldsymbol{q}} + \boldsymbol{g}(\boldsymbol{q}) = \boldsymbol{u} + \boldsymbol{\tau}_{\text{ext}} \tag{1}$$

with the joint angles given by $\boldsymbol{q} \in \mathbb{R}^n$. The symmetric and positive inertia matrix is denoted by $\boldsymbol{M}(\boldsymbol{q}) \in \mathbb{R}^{n\times n}$ and the Coriolis/centrifugal matrix by $\boldsymbol{C}(\boldsymbol{q},\dot{\boldsymbol{q}}) \in \mathbb{R}^{n\times n}$, while $\boldsymbol{g}(\boldsymbol{q}) \in \mathbb{R}^n$ represents the gravity torques.[1] The control input is given by $\boldsymbol{u} \in \mathbb{R}^n$ and the influence of external loads by $\boldsymbol{\tau}_{\text{ext}} \in \mathbb{R}^n$.

Initially, the coordinates $\boldsymbol{x}_i \in \mathbb{R}^{m_i}$ of the operational space tasks for all r levels of the hierarchy must be defined, in which m_i denotes the dimension of the i-th task. The corresponding velocities are described by the Jacobian matrices $\boldsymbol{J}_i \in \mathbb{R}^{m_i\times n}$:

$$\dot{\boldsymbol{x}}_i = \boldsymbol{J}_i\dot{\boldsymbol{q}} \qquad \forall i = 1\ldots r. \tag{2}$$

The most well known null space projector in force-torque-controlled robots is the *dynamically consistent* one [29], which maps lower-priority control actions onto the dynamically consistent null spaces of all higher-priority tasks. That way, dynamic decoupling is achieved such that a control action on a lower-priority level does not lead to operational space accelerations on the higher levels, neither statically (in a steady state) nor dynamically (during the transient). The standard formulation of this projector is

$$\boldsymbol{N}_i = \boldsymbol{I} - (\boldsymbol{J}_{i-1}^{\text{aug}})^T(\boldsymbol{J}_{i-1}^{\text{aug}})^{\boldsymbol{M}+,T} \tag{3}$$

where $\boldsymbol{I}$ is the identity matrix, $(\boldsymbol{J}_{i-1}^{\text{aug}})^{\boldsymbol{M}+}$ denotes the dynamically consistent pseudoinverse of $\boldsymbol{J}_{i-1}^{\text{aug}}$ (i.e. using the inertia matrix as metric for computing the pseudoinverse), and $\boldsymbol{J}_j^{\text{aug}}$ represents the so-called augmented Jacobian matrix

$$\boldsymbol{J}_j^{\text{aug}} = \begin{pmatrix} \boldsymbol{J}_1 \\ \vdots \\ \boldsymbol{J}_j \end{pmatrix} \tag{4}$$

which takes all Jacobian matrices down to level j into account. In [17], [18], we have introduced a mathematical formulation, which represents dynamic consistency [29] in hierarchically decoupled equations of motion. These decoupled dynamics are expressed in a set of local, hierarchy-consistent null space velocities $\boldsymbol{v}_1$ to $\boldsymbol{v}_r$, where

$$\underbrace{\begin{pmatrix} \boldsymbol{v}_1 \\ \vdots \\ \boldsymbol{v}_r \end{pmatrix}}_{\boldsymbol{v}} = \underbrace{\begin{pmatrix} \bar{\boldsymbol{J}}_1 \\ \vdots \\ \bar{\boldsymbol{J}}_r \end{pmatrix}}_{\bar{\boldsymbol{J}}} \dot{\boldsymbol{q}}. \tag{5}$$

The definition of the new Jacobian matrices $\bar{\boldsymbol{J}}_1$ to $\bar{\boldsymbol{J}}_r$ is given in the Appendix in (23) to (24) and will not be focused here. The overall control action for the realization of the task hierarchy is then

$$\boldsymbol{u} = \boldsymbol{g} + \sum_{i=1}^{r} \boldsymbol{u}_i \tag{6}$$

where the control action $\boldsymbol{u}_i$ from level i is

$$\boldsymbol{u}_i = -\boldsymbol{N}_i\boldsymbol{J}_i^T \underbrace{\left(\left(\frac{\partial V_i}{\partial \boldsymbol{x}_i}\right)^T + \boldsymbol{D}_i\dot{\boldsymbol{x}}_i\right)}_{\boldsymbol{F}_i} \tag{7}$$

[1] For the sake of simplicity, all dependencies will be dropped in the notations for the remainder of this letter.

for the case of an impedance-based control task with potential V_i and damping matrix $\boldsymbol{D}_i$ creating the task wrench $\boldsymbol{F}_i$. Note that $\boldsymbol{N}_1 = \boldsymbol{I}$ since the main task is not constrained.

Applying the coordinate transformation (5) to (1) leads to

$$\boldsymbol{\Lambda}\dot{\boldsymbol{v}} + \boldsymbol{\mu}\boldsymbol{v} + \begin{pmatrix} \boldsymbol{F}_1 \\ \boldsymbol{Z}_2\boldsymbol{J}_2^T\boldsymbol{F}_2 \\ \vdots \\ \boldsymbol{Z}_r\boldsymbol{J}_r^T\boldsymbol{F}_r \end{pmatrix} = \bar{\boldsymbol{J}}^{-T}\boldsymbol{\tau}_{\text{ext}} \tag{8}$$

with the null space base matrices $\boldsymbol{Z}_i$ as defined in the Appendix in (22). The transformed inertia matrix is denoted by $\boldsymbol{\Lambda}$ showing a block-diagonal structure while the transformed Coriolis/centrifugal matrix is given by $\boldsymbol{\mu}$. If all external wrenches are collocated to the task velocities $\dot{\boldsymbol{x}}_i$ then $\bar{\boldsymbol{J}}^{-T}\boldsymbol{\tau}_{\text{ext}} = \bar{\boldsymbol{J}}^{-T}(\boldsymbol{J}_r^{\text{aug}})^T\boldsymbol{F}_{\text{ext}}$ with $\boldsymbol{F}_{\text{ext}} \in \mathbb{R}^{\sum_{i=1}^{r} m_i}$ and $\bar{\boldsymbol{J}}^{-T}(\boldsymbol{J}_r^{\text{aug}})^T$ being an upper triangular matrix. In other words, the higher the priority level, the larger the influence by forces $\boldsymbol{F}_{\text{ext}}$ exerted on the robot in the operational spaces (2). This is counter-intuitive, because it is in contrast to the actual task hierarchy. Nevertheless, this is an inevitable direct result of the dynamic decoupling of the kinetic energies on all hierarchy levels introduced by the dynamic consistency [29].

B. Dynamic Model

The dynamics of a humanoid robot is usually described by a floating base model. Often one chooses either the hip or the trunk as base since both are central bodies of the structure of the robot. In [7], the authors suggested to use the CoM for legged robots instead, because the location of the CoM is crucial for balancing. Here, we will reuse this concept by defining a frame $\mathcal{C}$, which is located at the CoM and which has the same orientation as the hip of the robot. The frame is determined by the vector $\boldsymbol{x}_c \in \mathbb{R}^3$ (translation) and the rotation matrix $\boldsymbol{R}_c \in \mathbb{R}^{3\times3}$ with respect to the world frame $\mathcal{W}$. The corresponding translational and rotational velocities are given by $\dot{\boldsymbol{x}}_c$ and $\boldsymbol{\omega}_c \in \mathbb{R}^3$. Based on the joint angles $\boldsymbol{\theta} \in \mathbb{R}^n$ for the n actuated joints, the dynamics of a humanoid robot can be described by

$$\tilde{\boldsymbol{M}}\begin{pmatrix} \dot{\boldsymbol{\nu}}_c \\ \ddot{\boldsymbol{\theta}} \end{pmatrix} + \tilde{\boldsymbol{C}}\begin{pmatrix} \boldsymbol{\nu}_c \\ \dot{\boldsymbol{\theta}} \end{pmatrix} + \begin{pmatrix} m\boldsymbol{g}_0 \\ \boldsymbol{0} \end{pmatrix} = \underbrace{\begin{pmatrix} \boldsymbol{0} \\ \boldsymbol{\tau} \end{pmatrix}}_{\boldsymbol{u}} + \boldsymbol{\tau}_{\text{ext}} \tag{9}$$

with $\tilde{\boldsymbol{M}} \in \mathbb{R}^{(6+n)\times(6+n)}$ and $\tilde{\boldsymbol{C}} \in \mathbb{R}^{(6+n)\times(6+n)}$ being the inertia and Coriolis/centrifugal matrix, respectively. The velocities concerning the frame $\mathcal{C}$ are stacked into $\boldsymbol{\nu}_c = (\dot{\boldsymbol{x}}_c^T\ \boldsymbol{\omega}_c^T)^T$. The influence of gravity on the CoM is given by the overall mass m of the robot and the vector of gravitational acceleration $\boldsymbol{g}_0 \in \mathbb{R}^6$. The control input $\boldsymbol{u}$ consists of the joint torques $\boldsymbol{\tau} \in \mathbb{R}^n$ taking the underactuation of the base into account. The external loads acting on the robot are represented by $\boldsymbol{\tau}_{\text{ext}} \in \mathbb{R}^{6+n}$.

C. New Approach

The controller presented in this section implements a task hierarchy consisting of four different priority levels: the task with the highest priority utilizes a subset of the Ψ end effectors, namely the end effectors 1 to ψ with $\psi \leq \Psi$, for generating suitable contact wrenches in order to maintain balance. The contact wrenches of those balancing end effectors are stacked into $\boldsymbol{F}_{\text{bal}} = (\tilde{\boldsymbol{F}_1}^T, \ldots, \tilde{\boldsymbol{F}_\psi}^T)^T$. The second task comprises the remaining end effectors ($\psi + 1 \leq i \leq \Psi$), which can be used for interaction with the environment, for instance to perform a manipulation task. For this, each end effector $\psi + 1$ to Ψ is subject to virtual Cartesian compliance stabilizing the pose of the end effector relative to the world frame $\mathcal{W}$. Each compliance control is determined by a translational and rotational stiffness and damping matrix. The wrenches of the interaction end effectors are analogously combined to $\boldsymbol{F}_{\text{int}} = (\tilde{\boldsymbol{F}}_{\psi+1}^T, \ldots, \tilde{\boldsymbol{F}}_{\Psi}^T)^T$. The third-priority level is given by Cartesian compliance control which stabilizes the CoM location $\boldsymbol{x}_c$ and the hip orientation $\boldsymbol{R}_c$ relative to the world frame $\mathcal{W}$. Again, this compliance consists of a translational and rotation stiffness and damping term resulting in the desired CoM wrench $\boldsymbol{F}_c \in \mathbb{R}^6$. The task with the lowest priority is supposed to stabilize the posture of the robot in joint space in order to deal with redundant kinematics and singular configurations. The task generates a desired joint torque $\boldsymbol{\tau}_{\text{pose}}$ based on a compliance defined in joint space.

Applying (6) to the above task hierarchy leads to

$$\boldsymbol{u} = \begin{pmatrix} \boldsymbol{0} \\ \boldsymbol{\tau} \end{pmatrix} = \begin{pmatrix} m\boldsymbol{g}_0 \\ \boldsymbol{0} \end{pmatrix} - \underbrace{\begin{bmatrix} \boldsymbol{J}_{\text{bal}}^T \\ \boldsymbol{N}_2\boldsymbol{J}_{\text{int}}^T \\ \boldsymbol{N}_3\boldsymbol{J}_c^T \\ \boldsymbol{N}_4\boldsymbol{J}_{\text{pose}}^T \end{bmatrix}}_{\boldsymbol{\Xi} = \begin{bmatrix} \boldsymbol{\Xi}_u \\ \boldsymbol{\Xi}_l \end{bmatrix}} \underbrace{\begin{pmatrix} \boldsymbol{F}_{\text{bal}} \\ \boldsymbol{F}_{\text{int}} \\ \boldsymbol{F}_c \\ \boldsymbol{\tau}_{\text{pose}} \end{pmatrix}}_{\boldsymbol{F}} \tag{10}$$

with $\boldsymbol{J}_{\text{bal}}$, $\boldsymbol{J}_{\text{int}}$, $\boldsymbol{J}_c$ and $\boldsymbol{J}_{\text{pose}}$ being the corresponding task Jacobian matrices. In order to take the underactuation of the base into account, the contact wrenches $\boldsymbol{F}_{\text{bal}}$ of the balancing end effectors must be chosen such that

$$\boldsymbol{0} = m\boldsymbol{g}_0 - \boldsymbol{\Xi}_u\boldsymbol{F} \tag{11}$$

holds at all times.

If the robot uses more than one end effector for balancing then its kinematics can be split into a serial and a parallel part. The latter is represented by task 1 in the form of the kinematic loop of the balancing end effectors. The remaining tasks concern the serial part of the kinematics only. In consequence, the balancing wrenches $\boldsymbol{F}_{\text{bal}}$ cannot be directly obtained from (11) because (11) offers only 6 equations for the 6ψ DoF of $\boldsymbol{F}_{\text{bal}}$, which is also known as the wrench distribution problem ([3], [9]). In order to deal with this redundancy, $\boldsymbol{F}_{\text{bal}}$ can be determined instead via the following optimization problem

$$\min_{\boldsymbol{F}_{\text{bal}}} \left(\boldsymbol{F}_{\text{bal}} - \boldsymbol{F}_{\text{bal}}^d\right)^T \boldsymbol{Q} \left(\boldsymbol{F}_{\text{bal}} - \boldsymbol{F}_{\text{bal}}^d\right) \tag{12}$$

with respect to the constraints (11) and

$$\tilde{f}_{i,\perp} \geq \tilde{f}_i^{\min} \qquad \forall i = 1 \ldots \psi, \tag{13}$$

$$\left\| \tilde{\boldsymbol{f}}_{i,\parallel} \right\| \leq \mu_i \tilde{f}_{i,\perp} \qquad \forall i = 1 \ldots \psi, \tag{14}$$

$$\boldsymbol{p}_i(\tilde{\boldsymbol{F}}_i) \in \mathcal{S}_i \qquad \forall i = 1 \ldots \psi, \tag{15}$$

$$|\boldsymbol{\Xi}_l\boldsymbol{F}| \leq \boldsymbol{\tau}^{\max}. \tag{16}$$

TABLE I
DIFFERENT ORDERS WITHIN THE TASK HIERARCHY

Level i	"Int. over CoM"	"CoM over Int."
1	$\boldsymbol{F}_{\text{bal}}$	$\boldsymbol{F}_{\text{bal}}$
2	$\boldsymbol{F}_{\text{int}}$	$\boldsymbol{F}_c$
3	$\boldsymbol{F}_c$	$\boldsymbol{F}_{\text{int}}$
4	$\boldsymbol{\tau}_{\text{pose}}$	$\boldsymbol{\tau}_{\text{pose}}$

The cost function (12) minimizes the deviation of the end effector wrenches $\boldsymbol{F}_{\text{bal}}$ from a default wrench distribution $\boldsymbol{F}_{\text{bal}}^d$, which can be provided by an offline planer, for example. The weighting matrix $\boldsymbol{Q}$ is symmetric and positive definite. The constraints (13) to (15) represent the contact model by preventing each balancing end effector from lifting off, slipping and tilting: in here, $\tilde{f}_{i,\perp}$ and $\tilde{\boldsymbol{f}}_{i,\parallel}$ denote the components of $\tilde{\boldsymbol{f}}_i$ perpendicular and parallel to the contact surface $\mathcal{S}_i$. The unilaterality of the contact is taken into account by (13) by limiting the minimum contact force to $\tilde{f}_i^{\min} \geq 0$. In order to prevent the end effectors from slipping, $\tilde{\boldsymbol{f}}_{i,\parallel}$ is limited via the friction coefficient μ_i in (14). The CoP of each end effector $\boldsymbol{p}_i(\tilde{\boldsymbol{F}}_i)$ is restricted to $\mathcal{S}_i$ in order to prevent the end effectors from tilting (see (15)). The constraint (16) ensures that the resulting joint torques stay within the limitations $\boldsymbol{\tau}^{\max}$ of the hardware.

After computing the balancing wrenches $\boldsymbol{F}_{\text{bal}}$, the control torque

$$\boldsymbol{\tau} = -\boldsymbol{\Xi}_l \boldsymbol{F} \tag{17}$$

can be obtained from the lower set of equations in (10).

In the task hierarchy presented above, the interaction end effectors have a higher priority than the CoM task such that a motion of the CoM will not dynamically affect the interaction task. This can be motivated with a scenario, in which the robot is supposed to locomote while carrying an object as e.g. a glass of water. In the remainder of the letter, we will refer to this choice of task hierarchy as "Int. over CoM". But one can also think of ordering the tasks in a different way as e.g. in Table I. Here, the order "CoM over Int." suggests to swap the priority level of the CoM and the interaction end effectors. This variant is motivated by the fact that the CoM is crucial for balancing and thereby must not be disturbed by the interaction end effectors.

D. Constrained Reduced Dynamics

Let us assume that the optimization (12) to (16) can find a feasible solution $\boldsymbol{F}_{\text{bal}}$, then inserting (10) into (9) leads to the transformed closed-loop dynamics (8). Furthermore, let us assume that the balancing end effectors are in rigid contact with the environment leading to $\dot{\boldsymbol{v}}_1 = \boldsymbol{v}_1 = \boldsymbol{0}$ (see Table I). Thus, one can use the transformation

$$\begin{pmatrix} \boldsymbol{v}_1 \\ \boldsymbol{v}_2 \\ \boldsymbol{v}_3 \\ \boldsymbol{v}_4 \end{pmatrix} = \underbrace{\begin{bmatrix} \boldsymbol{0} & \boldsymbol{0} & \boldsymbol{0} \\ \boldsymbol{I} & \boldsymbol{0} & \boldsymbol{0} \\ \boldsymbol{0} & \boldsymbol{I} & \boldsymbol{0} \\ \boldsymbol{0} & \boldsymbol{0} & \boldsymbol{I} \end{bmatrix}}_{\boldsymbol{T}} \underbrace{\begin{pmatrix} \boldsymbol{v}_2 \\ \boldsymbol{v}_3 \\ \boldsymbol{v}_4 \end{pmatrix}}_{\boldsymbol{v}^*} \tag{18}$$

for removing $\boldsymbol{v}_1$, leading to the reduced closed-loop dynamics

$$\boldsymbol{\Lambda}^* \dot{\boldsymbol{v}}^* + \boldsymbol{\mu}^* \boldsymbol{v}^* + \begin{pmatrix} \boldsymbol{Z}_2 \boldsymbol{J}_{\text{int}}^T \boldsymbol{F}_{\text{int}} \\ \boldsymbol{Z}_3 \boldsymbol{J}_c^T \boldsymbol{F}_c \\ \boldsymbol{Z}_4 \boldsymbol{J}_{\text{pose}}^T \boldsymbol{\tau}_{\text{pose}} \end{pmatrix} = \boldsymbol{T}^T \bar{\boldsymbol{J}}^{-T} \boldsymbol{\tau}_{\text{ext}} \tag{19}$$

with $\boldsymbol{\Lambda}^* = \boldsymbol{T}^T \boldsymbol{\Lambda} \boldsymbol{T}$ and $\boldsymbol{\mu}^* = \boldsymbol{T}^T \boldsymbol{\mu} \boldsymbol{T}$. Note that the transformation preserves the block-diagonal structure of the inertia matrix. The decoupled dynamics (19) has the same form as used in [17], [18] to prove asymptotic stability of the equilibrium for the hierarchical multi-objective control.

E. Feasibility of the Wrench Distribution Problem

The optimization problem (12) can become infeasible if the necessary balancing wrench $\boldsymbol{F}_{\text{bal}}$ cannot be generated due to the contact model or the maximal joint torque. In order to render the optimization always feasible, one can formulate the task wrenches $\boldsymbol{F}_{\text{int}}$, $\boldsymbol{F}_c$ and $\boldsymbol{\tau}_{\text{pose}}$ as soft constraints as suggested in [9]. By choosing the corresponding weights much higher than $\boldsymbol{Q}$, the soft constraints will only be relaxed if $\boldsymbol{F}_{\text{bal}}$ can otherwise not be generated. The consequence is that the other task wrenches are no longer matching $\boldsymbol{F}_{\text{int}}$, $\boldsymbol{F}_c$ and $\boldsymbol{\tau}_{\text{pose}}$. But if they are only clipped without changing their orientation it might still be enough to stabilize the system. Note that the null space projectors in (10) implement a hierarchy for the serial kinematics of the robot. But is is also possible to define a second hierarchy for solving the force distribution problem: by choosing the weights of the soft constraints mentioned above, one can specify the order in which the optimization should give up the task wrenches $\boldsymbol{F}_{\text{int}}$, $\boldsymbol{F}_c$ and $\boldsymbol{\tau}_{\text{pose}}$ for generating $\boldsymbol{F}_{\text{bal}}$ despite the contact model and the maximum joint torque.

F. Link to the Balancing Approach [9]

The balancing controller presented in Sec. II-C is a combination of the hierarchical multi-task control [17] as recapitulated in Sec. II-A and of the passivity-based balancing approach [9]. The latter enables the robot to perform an interaction task while balancing on multiple contacts. The difference is that the approach in [9] does not offer a dynamic decoupling of the tasks or an embedded joint impedance $\boldsymbol{\tau}_{\text{pose}}$. Thus, the new approach can be simplified to [9] by setting the null space projectors in (10) to $\boldsymbol{N}_2 = \boldsymbol{I}$, $\boldsymbol{N}_3 = \boldsymbol{I}$ and $\boldsymbol{N}_4 = \boldsymbol{0}$. The closed-loop dynamics can be derived as

$$\tilde{\boldsymbol{M}} \begin{pmatrix} \dot{\boldsymbol{\nu}}_c \\ \ddot{\boldsymbol{\theta}} \end{pmatrix} + \tilde{\boldsymbol{C}} \begin{pmatrix} \boldsymbol{\nu}_c \\ \dot{\boldsymbol{\theta}} \end{pmatrix} + \begin{pmatrix} \boldsymbol{F}_c \\ \boldsymbol{0} \end{pmatrix} = -\boldsymbol{J}_{\text{bal}}^T \boldsymbol{F}_{\text{bal}} - \boldsymbol{J}_{\text{int}}^T \boldsymbol{F}_{\text{int}} + \boldsymbol{\tau}_{\text{ext}}. \tag{20}$$

In order to deal with kinematically redundant robots and singular configurations, we added a conventional null space controller to the torque of the balancer in [9] by

$$\boldsymbol{\tau} = -\boldsymbol{\Xi}_l \boldsymbol{F} + \boldsymbol{N}_{\text{null}} \boldsymbol{\tau}_{\text{pose}} \tag{21}$$

with $\boldsymbol{N}_{\text{null}} \in \mathbb{R}^{n \times n}$ being a null space projector w.r.t. $\begin{bmatrix} \boldsymbol{J}_{\text{bal}}^T & \boldsymbol{J}_{\text{int}}^T \end{bmatrix}^T$. The consequence is that the generated balancing wrenches can violate the contact model or the joint torque limits

TABLE II
PARAMETERS FOR THE BALANCING CONTROLLER

CoM:	
$\boldsymbol{K}_c = \mathrm{diag}(1500\,1500\,3000)^{\mathrm{N/m}}$	$\boldsymbol{D}_c = \mathrm{diag}(171\,102\,0)^{\mathrm{Ns/m}}$
$\boldsymbol{L}_c = \mathrm{diag}(200\,100\,100)^{\mathrm{Nm/rad}}$	$\boldsymbol{B}_c = \mathrm{diag}(15\,17\,10)^{\mathrm{Nms/rad}}$
FootR, FootL:	
$\tilde{f}_i^{\min} = 50\,\mathrm{N}$	$\tilde{\mu}_i = 0.4$
$p_{\mathrm{i,x}}^{\min} = -0.07\,\mathrm{m}$	$p_{\mathrm{i,x}}^{\max} = 0.13\,\mathrm{m}$
$p_{\mathrm{i,y}}^{\min} = -0.045\,\mathrm{m}$	$p_{\mathrm{i,y}}^{\max} = 0.045\,\mathrm{m}$
$\boldsymbol{Q}_i = \mathrm{diag}(10^{-3}\,10^{-3}\,10^{-3}\,1\,1\,1)$	
HandR, HandL:	
$\boldsymbol{K}_i = \mathrm{diag}(600, 600, 600)^{\mathrm{N/m}}$	$\boldsymbol{D}_i = \mathrm{diag}(10, 10, 10)^{\mathrm{Ns/m}}$
$\boldsymbol{L}_i = \mathrm{diag}(10, 10, 10)^{\mathrm{Nm/rad}}$	$\boldsymbol{B}_i = \mathrm{diag}(1, 1, 1)^{\mathrm{Nms/rad}}$
Joint Space:	
$\boldsymbol{K}_{\mathrm{pose}} = \mathrm{diag}(10\,\ldots\,10)^{\mathrm{Nm/rad}}$	$\boldsymbol{D}_{\mathrm{pose}} = \mathrm{diag}(1\,\ldots\,1)^{\mathrm{Nms/rad}}$

of the hardware since the conventional null space controller is added after the optimization of $\boldsymbol{F}_{\mathrm{bal}}$. In contrast to that, the balancing approach presented in this work has a built-in joint compliance in the form of task 4, whose desired torque $\boldsymbol{\tau}_{\mathrm{pose}}$ is already considered in the optimization and thereby in the inequality constraints (13) to (16).

III. EVALUATION

The experiments and simulations presented in this section were conducted with the humanoid robot TORO, developed by DLR (German Aerospace Center). It has 27 DoF (not counting the hands), a height of $1.74\,\mathrm{m}$ and a weight of $76.4\,\mathrm{kg}$ [30], [31]. In the examined cases, the robot uses the legs for balancing and the arms for performing the interaction task. The corresponding 25 joints are based on the technology of the DLR-KUKA LBR III (lightweight robot arm) and are operated in torque control mode [32]. The two remaining joints, located in the neck, are locked. The three evaluated controllers are implemented in Matlab/Simulink and executed at a rate of $1\,\mathrm{kHz}$. In order to simplify the implementation, the friction cone from (14) is approximated with a pyramid governed by $\left|\tilde{f}_{i,x}\right| \leq \tilde{\mu}_i \tilde{f}_{i,z}$ and $\left|\tilde{f}_{i,y}\right| \leq \tilde{\mu}_i \tilde{f}_{i,z}$. The contact surface $\mathcal{S}_i$ is assumed to be a rectangle due to the geometric shape of the feet of TORO, confining the CoP to $p_{i,x}^{\min} \leq p_{i,x} \leq p_{i,x}^{\max}$ and $p_{i,y}^{\min} \leq p_{i,y} \leq p_{i,y}^{\max}$. Thus, the optimization becomes a constrained quadratic problem, which is solved by using qpOASES [33].

Several simulations and experiments were conducted in order to compare the new hierarchical approach presented in Sec. II-C with the balancer from [9] (Sec. II-F) with respect to their dynamical and static behavior. We will refer to the balancer from [9] as "HRO-approach" after the authors. The parameterization used for both approaches is listed in Table II while Fig. 2 shows the setup for the simulations and the experiments.

The first pair of simulation and experiment was conducted in order to verify the dynamical decoupling offered by the hierarchical balancing approach. More precisely, the robot was subjected to a motion of the CoM frame $\mathcal{C}$ in order to evaluate the influence on the interaction task represented by the hands. According to the theory, the hierarchical approach with

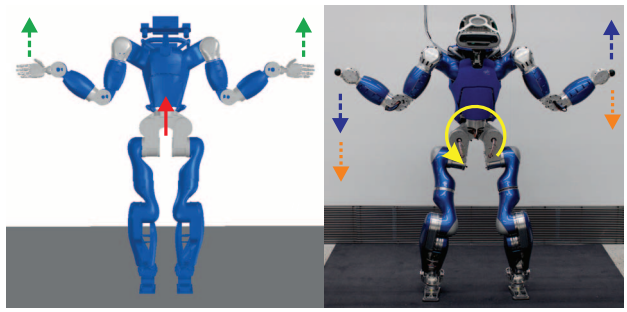

Fig. 2. Setup of the simulation (left): jump in the CoM position (red solid) and jump in the hand positions (green dashed). Setup of the experiment (right): trajectory of the CoM frame orientation (yellow solid), trajectory of the hand positions (blue dashed) and external wrenches (orange dotted).

the task order "Int. over CoM" should prevent the interaction tasks (hands) from being disturbed by the motion within the CoM task. In contrast to that, the hierarchical balancer "CoM over Int." should show a coupling from the level-2 task into the level-3 task as well as the "HRO-approach" (see Table I). For evaluation, one simulation was conducted in which a vertical jump in the desired CoM position of $0.05\,\mathrm{m}$ was commanded to the robot. As can be seen from Fig. 3, the hierarchical balancer "Int. over CoM" shows, as expected, a significantly smaller error in the position as well as in the orientation of the right hand. The performance of the hierarchical controller "CoM over Int." is worse than the "HRO-approach" but still comparable. Furthermore, one experiment was conducted in which a continuous trajectory was commanded to the robot rotating the CoM frame $\mathcal{C}$ as shown in Fig. 4. The trajectory consists of a sine with a frequency of $0.5\,\mathrm{Hz}$ and an amplitude which is linearly increased to $12°$, held constant and again decreased within $5\,\mathrm{s}$ each. As one can see from Fig. 4, the difference between the hierarchical balancer "Int. over CoM" and the "HRO-approach" is not as evident as in simulation. But both perform better than the controller "CoM over Int.".

The second pair of simulation and experiment was conducted to study the reverse dynamic influence by applying a motion at the hands (interaction task) and evaluating the control error in the CoM frame $\mathcal{C}$. Here, it is expected that the controller "CoM over Int." performs best due to the task hierarchy. For evaluation, a vertical jump of $0.1\,\mathrm{m}$ was commanded to the desired position of both hands in simulation. As can be seen from Fig. 5, the hierarchical approach "CoM over Int." shows a significantly smaller error than the other controllers for the location of the CoM. In the conducted experiment the right and left hand were complementarily moved up and down as shown in Fig. 2 in order to trigger a rotational motion of the CoM frame $\mathcal{C}$. The corresponding trajectory consists of a sine with a frequency of $0.6\,\mathrm{Hz}$ and an amplitude of $0.25\,\mathrm{m}$ which is increased, held constant, and decreased within $5\,\mathrm{s}$ each. As a result, the hierarchical approach "CoM over Int." performs best regarding the position error of the CoM. For the orientation of the CoM frame $\mathcal{C}$, all approaches show almost the same performance as can be seen in Fig. 6. The reason is that the inertial effect which the hands have on the torso of the robot is relatively small compared to joint friction.

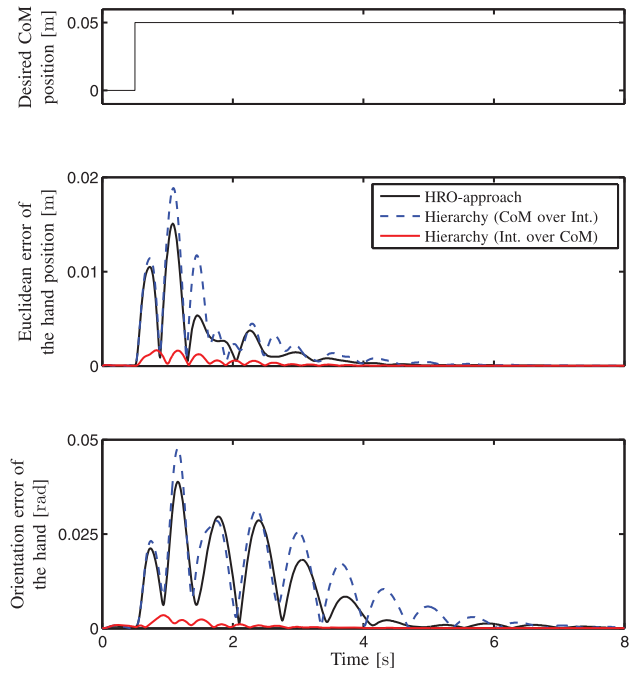

Fig. 3. Simulation on the responses to a step in the desired CoM position, evaluated at the right hand.

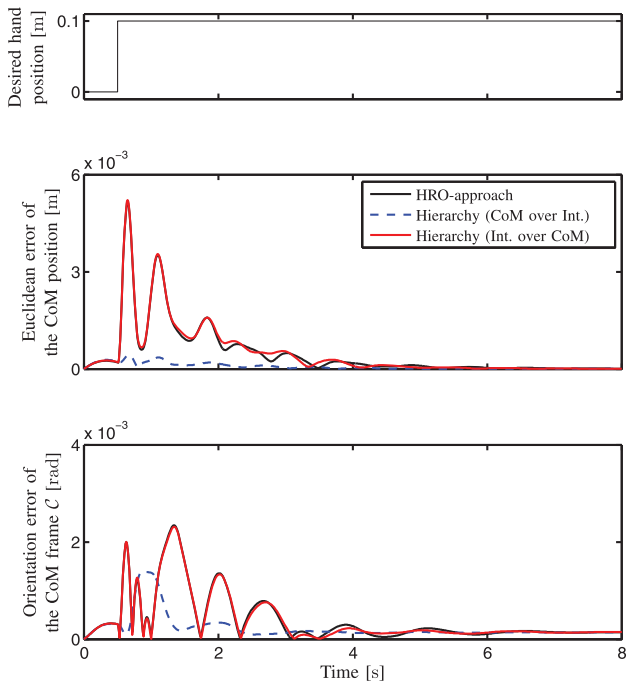

Fig. 5. Simulation on the responses to a step in the desired hand positions, evaluated at the CoM frame $\mathcal{C}$.

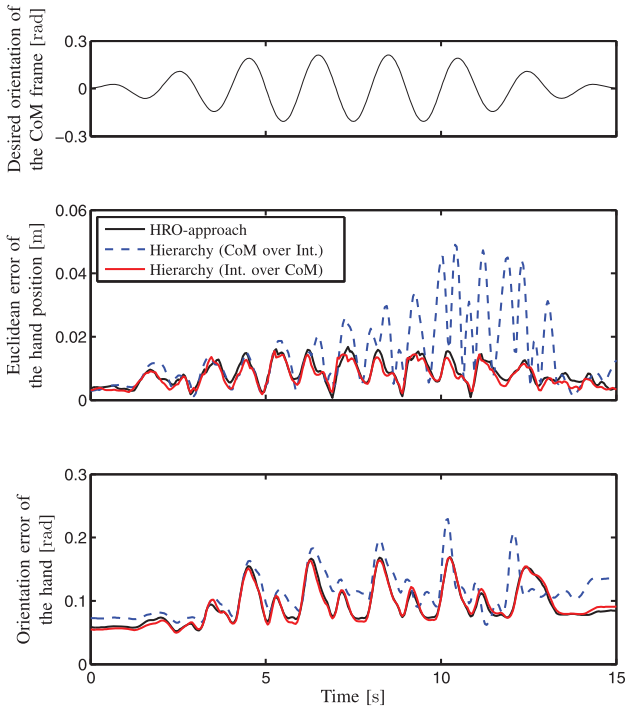

Fig. 4. Experiment on the responses to a trajectory of the desired orientation of the CoM frame $\mathcal{C}$, evaluated at the right hand.

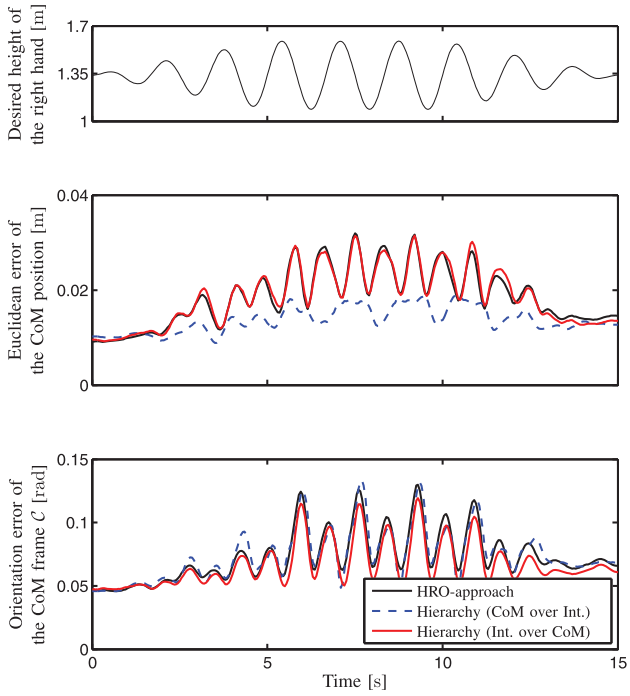

Fig. 6. Experiment on the responses to a trajectory of the desired hand positions, evaluated at the CoM frame $\mathcal{C}$.

The difference between experiment and simulation can be explained, for example, with modeling errors concerning the inertia matrix or with joint friction causing additional coupling between the CoM and the end effectors.

The last experiment was conducted in order to study the static influence of the interaction task onto the CoM frame $\mathcal{C}$. For this, additional weights of $5\,\mathrm{kg}$ were manually attached to the right and to the left hand each (see Fig. 2). The resulting transition for the deviation of the position and orientation of the CoM frame $\mathcal{C}$ is shown in Fig. 7. The "HRO-approach" and the task hierarchy "Int. over CoM" feature a comparable, good behavior. Their steady-state errors are negligible compared to the one of the hierarchical approach "CoM over Int.". In case of the "HRO-balancer", this observation can be explained with closed-loop behavior (20). Considering the static case, one can see from the second line of (20) that $\boldsymbol{\tau}_{\mathrm{ext}} = \left[\, \boldsymbol{J}_{\mathrm{bal}}^T \;\; \boldsymbol{J}_{\mathrm{int}}^T \,\right] \begin{pmatrix} \boldsymbol{F}_{\mathrm{bal}} \\ \boldsymbol{F}_{\mathrm{int}} \end{pmatrix}$

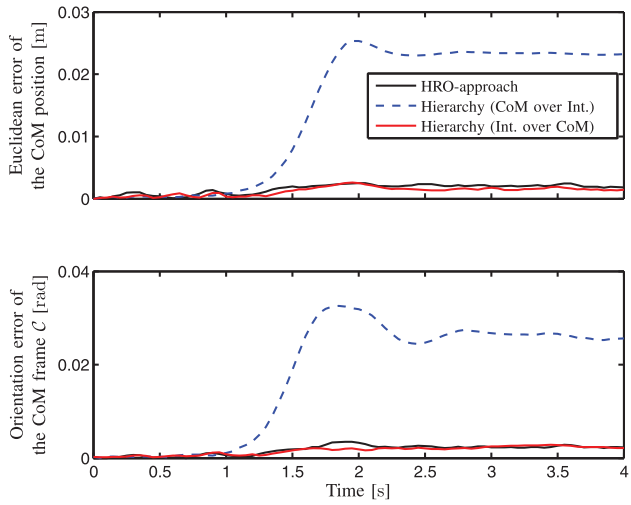

Fig. 7. Experiment on the influence on the CoM frame $\mathcal{C}$ due to external forces applied at the hands.

holds. Inserting this into the first line gives $\boldsymbol{F}_c = \mathbf{0}$ leading to a vanishing error in the pose of the CoM frame $\mathcal{C}$. In case of the hierarchical approach "CoM over Int." the observed behavior appears to be counter-intuitive at first glance because the CoM impedance has a higher priority than the Cartesian impedance of the hands. The reason for that behavior can be found in the mapping of the external forces and torques (8) represented by the upper triangular matrix $\bar{\boldsymbol{J}}^{-T}(\boldsymbol{J}_r^{\text{aug}})^T$. As described in Sec. II-A: the higher the priority level (lower index), the larger the influence by external forces exerted on the robot in the operational spaces (2). While this is counter-intuitive at first glance, since it contradicts the imposed task hierarchy, this is an inevitable consequence of dynamic decoupling of the priority levels. Due to the fact that the transmitted power is preserved along the transformation from task space to operational space (since it is just a coordinate transformation), the respective transformers are dual on the flow path (i.e. velocity) and the effort path (i.e. force/torque). As the dynamic decoupling is hierarchical, meaning that the higher-priority velocities are not affected by the lower-priority ones (which is the main goal of the hierarchical design), the mapping on the flow path is given by a lower triangular matrix. That, in turn, inevitably leads to the dual mapping on the effort path, i.e. the mentioned upper triangular mapping for forces/torques. Using the hierarchy "CoM over Int.", the external forces and torques exerted on the TCP have an impact on both levels, which yields the large steady-state errors in Fig. 7. On the contrary, in the hierarchy "TCP over CoM" such external loads only affect the main priority level but not the subordinate CoM impedance.

IV. Discussion

One advantage of the hierarchical approach over the "HRO-balancer" is the dynamically decoupled behavior due to the task prioritization. In fact, the dynamic equations related to the priority levels (8) are still coupled in terms of velocities via the matrix $\boldsymbol{\mu}$. Nevertheless, it has been shown in [18], that this coupling is negligible in practice for joint velocities during normal operation. Furthermore, stabilizing the robot in joint space is already embedded into the framework (see hierarchy level 4) and does not require an additional null space controller (21) as the "HRO-balancer". On the other hand the hierarchical approach requires the determination of the null space projectors (3).

The two examined hierarchies (Table I) are exemplary for two different kind of scenarios which a humanoid robot can typically encounter. The design for the hierarchy "CoM over Int." can be justified by the demand that a manipulation task should not compromise the CoM location, which is crucial for maintaining the balance in critical situations. On the other hand, it is important that a motion of the CoM, as for example during walking, does not interfere with the interaction task, such as carrying a glass of water. But the precision required for the interaction task is usually higher than the one for the CoM task, since the region in which the CoM must be located in order to enable a stable balancing is comparatively large. In consequence, it is recommendable to use the hierarchy "Int. over CoM" in conjunction with humanoid robots in most manipulation tasks. Another reason for choosing this particular hierarchy is that the CoM should not be statically affected by wrenches arising from the manipulation task. Regarding the experiment presented in Fig. 7, this feature is only provided by the "HRO-approach" and the hierarchal balancer "Int. over CoM".

V. Conclusions

This work presents a hierarchical whole-body controller for legged robots by combining a multi-objective controller with an optimization-based balancing approach capable of handling multiple contacts. It allows robust and compliant balancing of the robot while it performs a manipulation task in the presence of external disturbances. All tasks within the hierarchy generate generalized forces, which are distributed to the end effectors before being mapped to the joint torques. The approach was verified in simulation and experiment on the humanoid robot TORO, studying two representative setups for the choice of the task hierarchy. In summary, the new null-space-based approach "Int. over CoM" has clear advantages compared to the "HRO-balancer" because it reduces the dynamical influence of a CoM motion, as in walking, on the hands. Furthermore, it offers a decent disturbance rejection of the static external loads which arise during the manipulation task.

Appendix

The full row rank null space base matrix of $\boldsymbol{J}_{i-1}^{\text{aug}}$ is represented by

$$\boldsymbol{Z}_i = \begin{cases} \left(\boldsymbol{J}_1\boldsymbol{M}^{-1}\boldsymbol{J}_1^T\right)^{-1}\boldsymbol{J}_1\boldsymbol{M}^{-1} & \text{if } i=1 \\ \boldsymbol{J}_i\boldsymbol{Y}_{i-1}^T\left(\boldsymbol{Y}_{i-1}\boldsymbol{M}\boldsymbol{Y}_{i-1}^T\right)^{-1}\boldsymbol{Y}_{i-1} & \text{if } 1<i<r \\ \boldsymbol{Y}_{r-1} & \text{if } i=r \end{cases} \tag{22}$$

in which the matrix $\boldsymbol{Y}_{i-1} \in \mathbb{R}^{(n-\sum_{j=1}^{i-1} m_j)\times n}$ spans the complete null space of $\boldsymbol{J}_{i-1}^{\text{aug}}$ [18]. As detailed in [18], [34], the Jacobian matrix $\bar{\boldsymbol{J}}_i$ is defined as

$$\bar{\boldsymbol{J}}_1 = \boldsymbol{J}_1 \tag{23}$$

$$\bar{\boldsymbol{J}}_i = \left(\boldsymbol{Z}_i\boldsymbol{M}\boldsymbol{Z}_i^T\right)^{-1}\boldsymbol{Z}_i\boldsymbol{M} \qquad \forall 1<i\leq r. \tag{24}$$

ACKNOWLEDGEMENT

The authors would like to thank Robert Burger and Florian Schmidt for the support on the real-time software aspects related to the robot TORO.

REFERENCES

[1] B. J. Stephens and C. G. Atkeson, "Dynamic balance force control for compliant humanoid robots," in *Proc. IEEE/RSJ Int. Conf. Intell. Robots Syst.*, 2010, pp. 1248–1255.

[2] M. Mistry, J. Buchli, and S. Schaal, "Inverse dynamics control of floating base systems using orthogonal decomposition," in *Proc. IEEE Int. Conf. Robot. Autom.*, 2010, pp. 3406–3412.

[3] L. Righetti, J. Buchli, M. Mistry, M. Kalakrishnan, and S. Schaal, "Optimal distribution of contact forces with inverse-dynamics control," *Int. J. Robot. Res.*, vol. 32, no. 3, pp. 280–298, 2013.

[4] P. M. Wensing, G. B. Hammam, B. Dariush, and D. E. Orin, "Optimizing foot centers of pressure through force distribution in a humanoid robot," *Int. J. Humanoid Robot.*, vol. 10, no. 3, 1350027, 2013.

[5] L. Sentis, J. Park, and O. Khatib, "Compliant control of multicontact and center-of-mass behaviors in humanoid robots," *IEEE Trans. Robot.*, vol. 26, no. 3, pp. 483–501, Jun. 2010.

[6] A. Herzog, N. Rotella, S. Mason, F. Grimminger, S. Schaal, and L. Righetti, "Momentum control with hierarchical inverse dynamics on a torque-controlled humanoid," *Auton. Robots*, pp. 1–19, Aug. 2015.

[7] S.-H. Hyon, J. G. Hale, and G. Cheng, "Full-body compliant human-humanoid interaction: Balancing in the presence of unknown external forces," *IEEE Trans. Robot.*, vol. 23, no. 5, pp. 884–898, Oct. 2007.

[8] C. Ott, M. A. Roa, and G. Hirzinger, "Posture and balance control for biped robots based on contact force optimization," in *Proc. IEEE-RAS Int. Conf. Humanoid Robots*, 2011, pp. 26–33.

[9] B. Henze, M. A. Roa, and C. Ott, "Passivity-based whole-body balancing for torque-controlled humanoid robots in multi-contact scenarios," *Int. J. Robot. Res.*, 2015, submitted for publication.

[10] B. Paden and R. Panja, "Globally asymptotically stable 'PD+' controller for robot manipulators," *Int. J. Control*, vol. 47, no. 6, pp. 1697–1712, 1988.

[11] O. Kanoun, F. Lamiraux, and P.-B. Wieber, "Kinematic control of redundant manipulators: Generalizing the task-priority framework to inequality task," *IEEE Trans. Robot.*, vol. 27, no. 4, pp. 785–792, Aug. 2011.

[12] A. Escande, N. Mansard, and P.-B. Wieber, "Hierarchical quadratic programming: Fast online humanoid-robot motion generation," *Int. J. Robot. Res.*, vol. 33, no. 7, pp. 1006–1028, Jun. 2014.

[13] J. Baillieul, J. M. Hollerbach, and R. Brockett, "Programming and control of kinematically redundant manipulators," in *Proc. 23rd IEEE Conf. Decision Control*, Dec. 1984, pp. 768–774.

[14] Y. Nakamura, H. Hanafusa, and T. Yoshikawa, "Task-priority based redundancy control of robot manipulators," *Int. J. Robot. Res.*, vol. 6, no. 2, pp. 3–15, Jun. 1987.

[15] J. H. Hollerbach and K. C. Suh, "Redundancy resolution of manipulators through torque optimization," *IEEE J. Robot. Autom.*, vol. RA-3, no. 4, pp. 308–316, Aug. 1987.

[16] A. Dietrich, C. Ott, and A. Albu-Schäffer, "An overview of null space projections for redundant, torque-controlled robots," *Int. J. Robot. Res.*, vol. 34, no. 11, pp. 1385–1400, Sep. 2015.

[17] A. Dietrich, C. Ott, and A. Albu-Schäffer, "Multi-objective compliance control of redundant manipulators: Hierarchy, control, and stability," in *Proc. IEEE/RSJ Int. Conf. Intell. Robots Syst.*, Nov. 2013, pp. 3043–3050.

[18] C. Ott, A. Dietrich, and A. Albu-Schäffer, "Prioritized multi-task compliance control of redundant manipulators," *Automatica*, vol. 53, pp. 416–423, Mar. 2015, doi: 10.1016/j.automatica.2015.01.015.

[19] C. Ott, Cartesian Impedance Control of Redundant and Flexible-Joint Robots. New York, NY, USA: Springer, 2008, vol. 49.

[20] E. Marchand, F. Chaumette, and A. Rizzo, "Using the task function approach to avoid robot joint limits and kinematic singularities in visual servoing," in *Proc. IEEE/RSJ Int. Conf. Intell. Robots Syst.*, Nov. 1996, pp. 1083–1090.

[21] H. Sugiura, M. Gienger, H. Janssen, and C. Goerick, "Reactive self collision avoidance with dynamic task prioritization for humanoid robots," *Int. J. Humanoid Robot.*, vol. 7, no. 1, pp. 31–54, 2010.

[22] A. Dietrich, T. Wimböck, A. Albu-Schäffer, and G. Hirzinger, "Integration of reactive, torque-based self-collision avoidance into a task hierarchy," *IEEE Trans. Robot.*, vol. 28, no. 6, pp. 1278–1293, Dec. 2012.

[23] L. Sentis and O. Khatib, "Synthesis of whole-body behaviors through hierarchical control of behavioral primitives," *Int. J. Humanoid Robot.*, vol. 2, no. 4, pp. 505–518, Jan. 2005.

[24] O. Khatib, L. Sentis, J. Park, and J. Warren, "Whole-body dynamic behavior and control of human-like robots," *Int. J. Humanoid Robot.*, vol. 1, no. 1, pp. 29–43, Mar. 2004.

[25] H. Sadeghian, L. Villani, M. Keshmiri, and B. Siciliano, "Task-space control of robot manipulators with null-space compliance," *IEEE Trans. Robot.*, vol. 30, no. 2, pp. 493–506, Apr. 2014.

[26] A. Dietrich, T. Wimböck, A. Albu-Schäffer, and G. Hirzinger, "Reactive whole-body control: Dynamic mobile manipulation using a large number of actuated degrees of freedom," *IEEE Robot. Autom. Mag.*, vol. 19, no. 2, pp. 20–33, Jun. 2012.

[27] A. Dietrich *et al.*, "Whole-body impedance control of wheeled mobile manipulators: Stability analysis and experiments on the humanoid robot Rollin' Justin," *Auton. Robots*, pp. 1–13, 2015, doi: 10.1007/s10514-015-9438–z.

[28] F. L. Moro, M. Gienger, A. Goswami, N. G. Tsagarakis, and D. G. Caldwell, "An attractor-based whole-body motion control (WBMC) system for humanoid robots," in *Proc. 13th IEEE-RAS Int. Conf. Humanoid Robots*, Oct. 2013, pp. 42–49.

[29] O. Khatib, "A unified approach for motion and force control of robot manipulators: The operational space formulation," *IEEE J. Robot. Autom.*, vol. RA-3, no. 1, pp. 43–53, Feb. 1987.

[30] B. Henze, A. Werner, M. A. Roa, G. Garofalo, J. Englsberger, and C. Ott, "Control applications of TORO—a torque controlled humanoid robot," in *Proc. IEEE-RAS Int. Conf. Humanoid Robots*, Nov. 2014, p. 841.

[31] J. Englsberger *et al.*, "Overview of the torque-controlled humanoid robot TORO," in *Proc. IEEE-RAS Int. Conf. Humanoid Robots*, Madrid, Spain, Nov. 2014, pp. 916–923.

[32] A. Albu-Schäffer, C. Ott, and G. Hirzinger, "A unified passivity-based control framework for position, torque and impedance control of flexible joint robots," *Int. J. Robot. Res.*, vol. 26, no. 1, pp. 23–39, 2007.

[33] H. J. Ferreau, H. G. Bock, and M. Diehl, "An online active set strategy to overcome the limitations of explicit MPC," *Int. J. Robust Nonlinear Control*, vol. 18, no. 8, pp. 816–830, 2008.

[34] A. Dietrich, "Whole-body impedance control of wheeled humanoid robots," Ph.D. dissertation, Dept. Informat., Technische Universität München, Munich, Germany, 2015.